Heliyon 10 (2024) e28442

Contents lists available at ScienceDirect

Heliyon

journal homepage: www.cell.com/heliyon

Research article

# A clinical prognostic model of oxidative stress-related genes linked to tumor immune cell infiltration and the prognosis of ovarian cancer patients

Li Li [a,1], Weiwei Zhang [a,1], Yanjun Sun [a,b,1], Weiling Zhang [a,c], Mengmeng Lu [a,d], Jiaqian Wang [a,e], Yunfeng Jin [a,**], Qinghua Xi [a,*]

[a] Department of Obstetrics and Gynecology, Affiliated Hospital of Nantong University, Nantong, Jiangsu, 226001, China
[b] Department of Obstetrics and Gynecology, Affiliated Hospital of Nantong University, Medical School of Nantong University, Nantong, Jiangsu, 226001, China
[c] Department of Gynecology, Nantong Geriatric Rehabilitation Hospital, Nantong, Jiangsu, 226001, China
[d] Department of Obstetrics and Gynecology, Binhai County People's Hospital, Yancheng, Jiangsu, 224599, China
[e] Department of Obstetrics and Gynecology, Qidong Maternal and Child Health Hospital, Nantong, Jiangsu, 226200, China

ARTICLE INFO

*Keywords:*
Ovarian cancer
Oxidative stress
WGCNA
Unsupervised cluster analysis

ABSTRACT

*Background:* According to statistics, ovarian cancer (OV) is the most prevalent type of gynecologic malignancy and has the highest mortality rate of all gynecologic tumors. Although several studies have shown that oxidative stress (OS) contributes significantly to the onset and progression of cancer, the role of OS in OV needs to be investigated further. Thus, it is critical to comprehend the function of OS-related genes in OV.

*Methods:* In this study, all data related to the transcriptome and clinical status of the patients were retrieved from "The Cancer Genome Atlas" (TCGA) and "Gene Expression Omnibus" (GEO) databases. Using the unsupervised cluster analysis technique, all patients with OV were classified into two different subtypes (categories) based on the OS gene. All hub genes were screened using the weighted gene co-expression network analysis (WGCNA). Since the hub genes and the differentially expressed genes (DEGs) in both categories were found to intersect, the univariate Cox regression analysis was implemented. A multivariate Cox analysis was also performed to construct a novel clinical prognosis model, which was validated using data from the GEO cohort. In addition, the relationship between risk score and immune cell infiltration level was evaluated using CIBERSORT. Finally, qRT-PCR was used to confirm the expression of the genes used to construct the model.

*Results:* Two subtypes of OS were obtained. The findings indicated that OS-C1 had a better survival outcome than OS-C2. The results of WGCNA yielded 112 hub genes. For univariate COX regression analyses, 49 OS-related trait genes were obtained. Finally, a clinical prognostic model containing two genes was constructed. This model could differentiate between patients with OV having varying years of survival in the TCGA and GEO cohorts. The model risk score was verified as an independent prognostic indicator. According to the results of CIBERSORT, many tumor-infiltrating immune cells were found to be significantly related to the risk score. Furthermore,

* Corresponding author.
** Corresponding author.
*E-mail addresses:* jinyunfeng2016@126.com (Y. Jin), xiqinghua@ntu.edu.cn (Q. Xi).
[1] These authors contribute equally to this work.

https://doi.org/10.1016/j.heliyon.2024.e28442
Received 29 November 2023; Received in revised form 3 March 2024; Accepted 19 March 2024
Available online 21 March 2024

the results revealed that patients with low-risk OV in the CTLA4 treatment group had a high likelihood of benefiting from immunotherapy. qRT-PCR results also showed that the expression of *MARVELD1* and *VSIG4* was high in the OV samples.
*Conclusions:* Analysis of the results suggested that the newly developed model, which contained two characteristic OS-related genes, could successfully predict the survival outcomes of all patients with OV. The findings of this study could offer valuable information and insights into the refinement of personalized therapy and immunotherapy for OV in the future.

## 1. Introduction

Ovarian cancer (OV) is one of the most common types of gynecologic malignancies ranking fourth in terms of overall incidence. OV is characterized by frequent recurrences, metastasis, and drug resistance. It has the highest mortality rate among gynecological tumors [1–3]. OV has the second highest mortality rate among gynecological tumors in Chinese patients [4]. More importantly, since there are no early typical symptoms or effective early diagnosis methods, about 70% of patients with OV are already in their advanced stages when they are diagnosed. Also, more than 70% of patients experience a disease relapse after treatment [1]. Therefore, it is crucial to study OV pathogenesis and identify novel predictive molecular biomarkers for improving the diagnosis and therapeutic strategies for OV treatment.

Oxidative stress (OS) is caused by an imbalance between the production of reactive metabolites (including oxidants like reactive nitrogen species (RNS) and reactive oxygen species (ROS)) or free radicals and the antioxidant defense mechanisms of the human body. This imbalance can damage the biological molecules and tissues, and have an overall cumulative effect [5,6]. Increased oxidant production stimulates the antioxidant defense system, resulting in an OS state, which can cause irreversible and oxidative damage to the biomolecules like lipids, proteins, and nucleic acids [7–9]. These lesions are closely linked to the onset and advancement of cancer [10–12]. Previous studies have demonstrated that OS plays a significant role in cancer progression [6,13]. The ROS or RNS may promote genetic changes at the molecular level, which in turn can enhance the onset and advancement of tumors and further augment their resistance to therapy. Increased levels of ROS or RNS in the long term could have cytotoxic effects and activate the apoptotic pathways [14–17]. Studies have shown that iron and its metabolites promote ROS production through the Fenton reaction. During the formation of the chocolate cyst, the old blood in the ovary contains an extremely high iron content, which can enhance ROS production and induce DNA damage, increasing the risk of the malignant conversion from endometriosis to clear cell ovarian carcinoma [18]. The hydroxyl radicals produced by $H_2O_2$ in the Fenton reaction enhance the transferrin receptor-1 (TfR1) axis, which can cause multiple double-strand breaks in the DNA of epithelial cells of the oviduct, thereby promoting OV [19–21]. The relationship between OV and OS has gained a lot of research interest in the past few years. In addition, OS affects various immune cells such as tumor-associated macrophages, neutrophils, myeloid-derived suppressor cells, and regulatory T cells, and overall, altered oxidative stress may play an important role in sustaining the development of ovarian cancer cells [22,23]. However, the prognostic value of these OS genes in OV is still largely unclear, and more research is required to explore their potential mechanisms of action.

Using The Cancer Genome Atlas (TCGA) dataset, we aimed to reveal the genetic alterations and expression patterns of OS-related genes in OV, thereby revealing the molecular basis of OS involvement in this malignancy. Through rigorous bioinformatics analysis, we categorized OV samples into OS-high and OS-low groups to identify differentially expressed genes (DEGs) associated with OS risk profiles. A prognostic model was constructed based on a subset of these genes, demonstrating the potential to predict patient survival. In addition, we examined the tumor microenvironment (TME), immune cell infiltration, and drug sensitivity in the OV population in the OS high and OS low groups, providing insights into the clinical significance of OS-related gene expression. The findings of this study not only contribute to a better understanding of the OS-OV axis, but also provide a potential framework for personalized medicine in OV. By filling critical gaps in the knowledge of OS-related gene mechanisms, our study points to improved diagnostic and therapeutic strategies for patients with OV, with the ultimate goal of improving patient prognosis.

## 2. Materials and methods

### 2.1. Data collection and data processing

The mRNA expression profiles and clinical data for 381 OV tissues were obtained from TCGA (https://portal.gdc.cancer.gov/). The mRNA expression data of 88 healthy patients were acquired from the Genotype-Tissue Expression (GTEx) portal (https://gtexportal.org/home/datasets). The "sva" and "limma" R packages were used to remove any batch effects [24,25]. The list of OS-linked genes was acquired from the Amigo database (http://amigo.geneontology.org/). The GSE49997 dataset was retrieved from the Gene Expression Omnibus (GEO) (https://www.ncbi.nlm.nih.gov/geo/) as an authentication queue. The GSE49997 dataset contains 204 cancer samples, of which 10 samples lacking survival information were removed and the remaining 194 cancer samples were included in subsequent analyses. In addition, the TCGA database was used to obtain the copy number variation (CNV) and somatic data of patients with OV.

### 2.2. Unsupervised clustering analysis based on OS-linked genes in the OV cohort

The "CONSENSUS ClusterPlus" R package was used for unsupervised clustering analysis based on the OS-related genes. The "limma" R software was used to identify the DEGs across different categories, with a threshold of logfc = 1, $P < 0.05$.

### 2.3. Functional enrichment analysis and single sample gene set enrichment analysis algorithm (ssGSEA)

The R software "clusterProfiler" was used to assess the probable molecular functions, cellular components, biological processes, and KEGG (Kyoto Encyclopedia of Genes and Genomes) pathways of DEGs identified across different OS clusters [26]. To determine various KEGG approaches, the GSEA software was used to perform the GSEA analysis between high-risk and low-risk OV groups. The "C2. cp. kegg. v6.2. symbols" was acquired from the MSigDB database. Standardized enrichment fractions and nominal p-values were determined to analyze enrichment levels and the statistical significance. Moreover, the relationship between the infiltration abundance of 23 immune cells and different OS clusters was determined using the ssGSEA algorithm.

### 2.4. Weighted gene Co-expression network analysis (WGCNA)

It was noted that WGCNA could be used to classify genes into various modules based on the correlation between the genes in the microarray. The central or characteristic gene in the module can be used to classify the module. This method can also be used to associate modules with feature samples to identify the modules that are most relevant to targeted therapy or biomarkers [27]. The WGCNA algorithm could filter out the power value in the module construction. The gradient method was used to test the average connectivity and independence of various modules with varying power values. The appropriate efficiency value was determined when the degree of independence is 0.8. After determining the power value, the module was constructed using the WGCNA algorithm, and the information about the genes corresponding to each module was extracted. The minimum number of genes was set to 40. The co-expression module refers to a set of genes that have high similarity in topographical overlap. It was found that the genes within the same module had a higher degree of co-expression. The gene characteristic of a module denotes its first principal component and can be used to describe its expression profile in every sample. Finally, the correlation between the clinical data and the module was computed to obtain important clinical modules.

### 2.5. Construction and validation of clinical prognosis model

The intersection of the hub genes obtained from WGCNA analysis and the DEGs were analyzed to identify the characteristic OS-related genes. OS-related feature genes were uploaded to the STRING database to generate PPI networks [28]. The results of the PPI networks were visualized by the Cytoscape software and the scores of these nodes were calculated and ranked by the Cytohubba plugin. Next, the univariate regression analysis was employed to identify the characteristic OS-related genes with prognostic value. Finally, the multivariate regression model was used to identify the characteristic genes that could be used to build a clinical prognosis model. The following formula was used for clinical prognostic gene characteristics: Riskscore = (the expression of gene1 * Coef 1) + (the expression of gene2 * Coef 2) + (the expression of gene3 * Coef 3) + … + (the expression of geneN * Coef N), where Coef denotes a regression coefficient.

Thereafter, patients in the TCGA-OV group were classified into high-risk and low-risk groups based on their risk score values. The Kaplan-Meier (KM) curves were used to compare the survival rates of the two groups. Heatmaps were used to assess the gene expression levels used to construct the clinical prognosis models in the two groups. Furthermore, the area under the ROC curve (AUC) was employed to evaluate the prognostic value of the newly constructed model. Finally, the validation group was subjected to the same analysis to confirm the prediction ability of the clinical prognosis model.

### 2.6. Analysis of TME infiltration and somatic mutation in different risk groups

The CIBERSPORT algorithm was used to evaluate the relationship between risk scores and immune cell infiltration levels. The "maftools" R software was used to analyze the data for somatic variation [29]. Mutations in the high-risk and low-risk OV patient groups were visualized using the Waterfall diagram.

### 2.7. scRNA-seq data processing and analysis

For the single-cell dataset GSE154600, we first performed quality control to filter out low-quality cells. Then, normalization was performed using the default parameters of the Seurat "NormalizedData" function. The function FindVariableFeatures() was used to extract the first 2000 highly variable genes. ElbowPlot was used to define the most important principal component (PC) values in cell clustering, followed by UMAP analysis and clustering. To identify cell types, we used SingleR for automatic annotation.

### 2.8. Quantitative reverse transcription-polymerase chain reaction (qRT-PCR)

Total RNA was extracted from normal tissue and tumor tissue from patients using TRIzol reagent (Sigma-Aldrich, USA). Quantitative reverse transcription-polymerase chain reaction (qRT-PCR) was conducted on the obtained RNA from each sample. The cDNA

was utilized as a template with a reaction volume of 20 μl. Three separate analyses were performed on each sample. Based on the $2^{-\Delta\Delta CT}$ method, data from the threshold cycle (CT) were obtained and standardized to the levels of glyceraldehyde 3-phosphate dehydrogenase (GAPDH) in each sample. The following is a list of the sequences of primer pairs for the genes that were being targeted:

| Gene | Forward primer sequence (5-3) | Reverse primer sequence (5-3) |
|---|---|---|
| *MARVELD1* | GGTTTGTCAACGGTGCTGTC | CAAGGCCAGAATGGTGTTGC |
| *VSIG4* | AGAGAGTGTAACAGGACCTT | GTCACGTAGAAAGATGGTGA |
| *GAPDH* | AATGGGCAGCCGTTAGGAAA | GCCCAATACGACCAAATCAGAG |

### 2.9. Statistical analysis

The statistical analyses in this study were conducted using the R software (ver. 4.2.1). The Wilcoxon test was performed to compare the expression levels of immune checkpoint-associated genes and human leukocyte antigens in two different OS clusters. Furthermore, log-rank tests and KM analysis were used to assess the survival differences of patients in different groups. Pearson correlation analysis was employed to assess the correlation. The R tools "survival rate" and "time ROC" were used for ROC curve analysis. A value of $P < 0.05$ was seen as statistically significant.

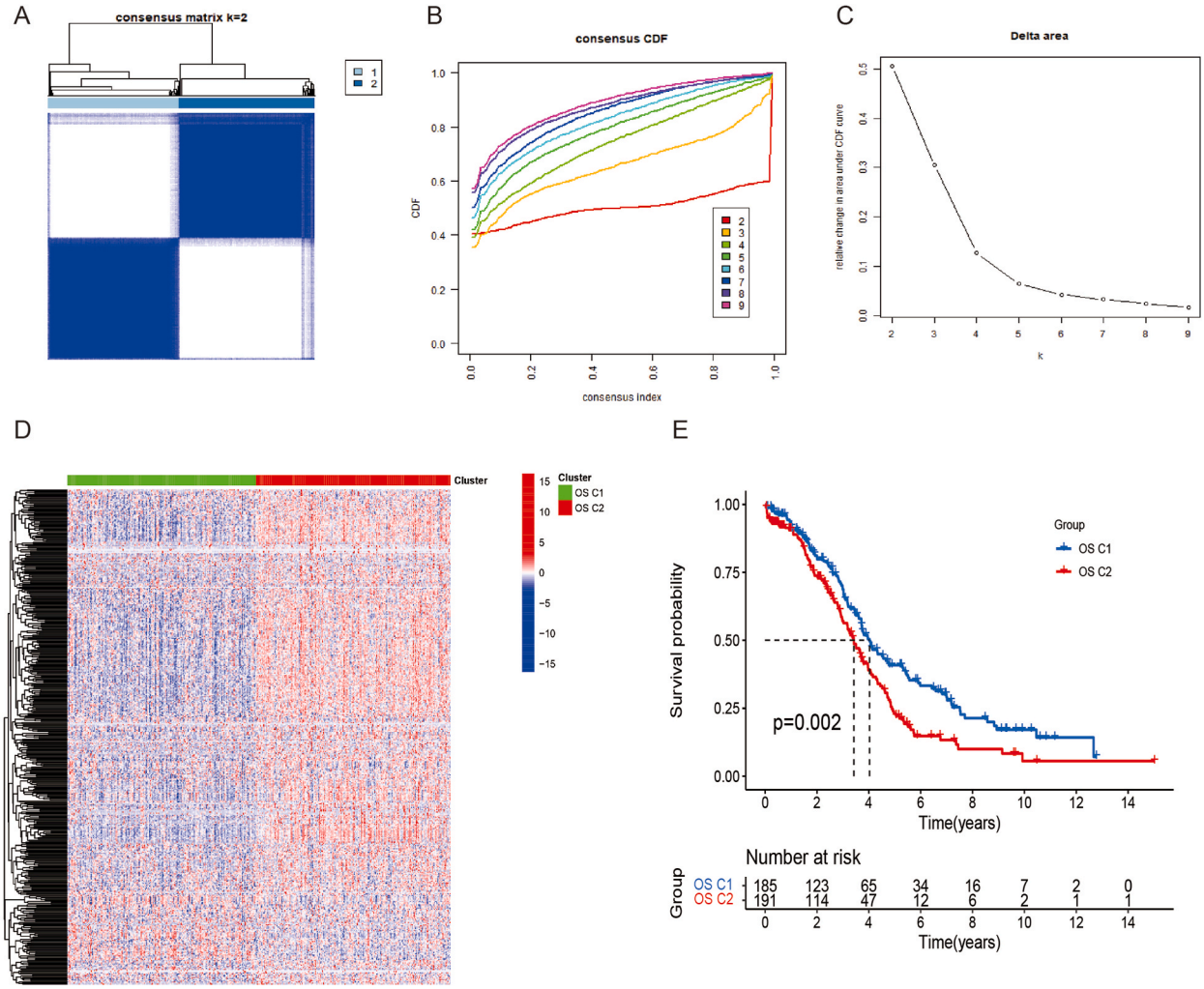


**Fig. 1.** Identification of OS related subtypes. (A–C) Using a consistent clustering algorithm, OV samples are divided into two different OS related subtypes, OS C1 and OS C2. C. Consistency matrix; D. CDF diagram; E. Relative change of area under CDF curve when k = 2–9. F. (D) The heat map shows the expression level of OS gene between OS C1 and OS C2.€) Survival analysis between OS C1 and OS C2.

## 3. Results

### 3.1. Identifying two different OS-linked subtypes in OV

The OS gene expression from the TCGA-OV cohort was extracted. Based on this data, the unsupervised cluster analysis was used to categorize the genes into two different OS-related categories, namely OS C1 and OS C2. (Fig. 1A–C). The differential expression levels of the OS-related genes in OS C1 and OS C2 categories were shown in the heatmap (Fig. 1D). The survival analysis highlighted the significant survival differences between the two categories. The findings revealed that the values of OS in the OS C2 group were lower than those in the OS C1 group (P = 0.002) (Fig. 1E).

### 3.2. Differential gene expression (DGE) analysis and function enrichment analysis of both OS-related subtypes

The DEGs between the two categories were compared, and functional analysis was performed to determine their probable signaling

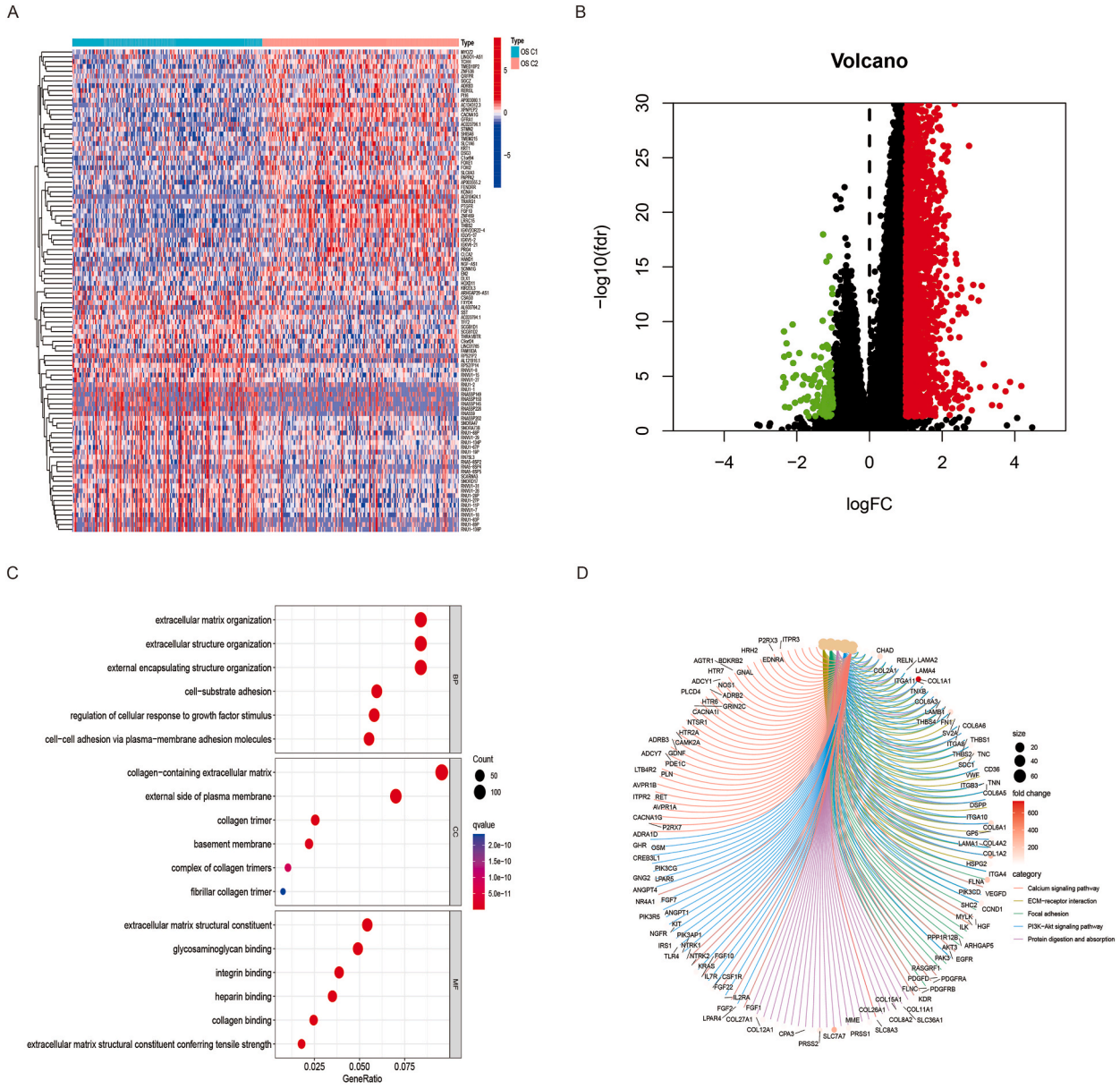


**Fig. 2.** Function enrichment analysis between OS C1 and OS C2. (A–B) Thermal and volcanic maps show the DEGs between OS C1 and OS C2. A: Heat map; B: Volcanic m€ (C) GO enrichment analysis. (D) KEGG pathway enrichment analysis.

pathways. The analysis yielded a total of 2573 DEGs (Fig. 2A and B). The findings of GO enrichment analysis revealed that the pathways involved in the external packaging of structural tissue, extracellular matrix (ECM) tissue, extracellular structure tissue, collagen-containing extracellular matrix, and the outside of plasma membrane, were significantly enriched in the DEGs (Fig. 2C). Results of the KEGG analysis showed that the PI3K-Akt signaling pathway, calcium signaling pathway, and other pathways related to focal induction, ECM-receiver interaction, protein digestion, and absorption, were significantly enriched in these DEGs (Fig. 2D).

### 3.3. Differences in immune cell infiltration and gene expression levels associated with immunotherapy between both OS categories

The GSEA analysis was performed to compare the enrichment of biological pathways between the two OS subgroups. The results showed that several pathways including those of myocardial contraction, Huntington's disease, juvenile diabetes mellitus, oxidative phosphorylation, and ribosome were enriched significantly in the OS C1 group (Fig. 3A). On the other hand, pathways for calcium signaling, cell adhesion molecule (CAM), ECM receptor interaction, focal adhesion, and neural active ligand-receptor interaction were significantly enriched in the OS C2 group (Fig. 3B). Significant differences were noted between the immune scores, matrix scores, estimated scores, and tumor purity of both OS categories. The stromal scores ($P < 0.001$), immune scores ($P < 0.01$), and estimated

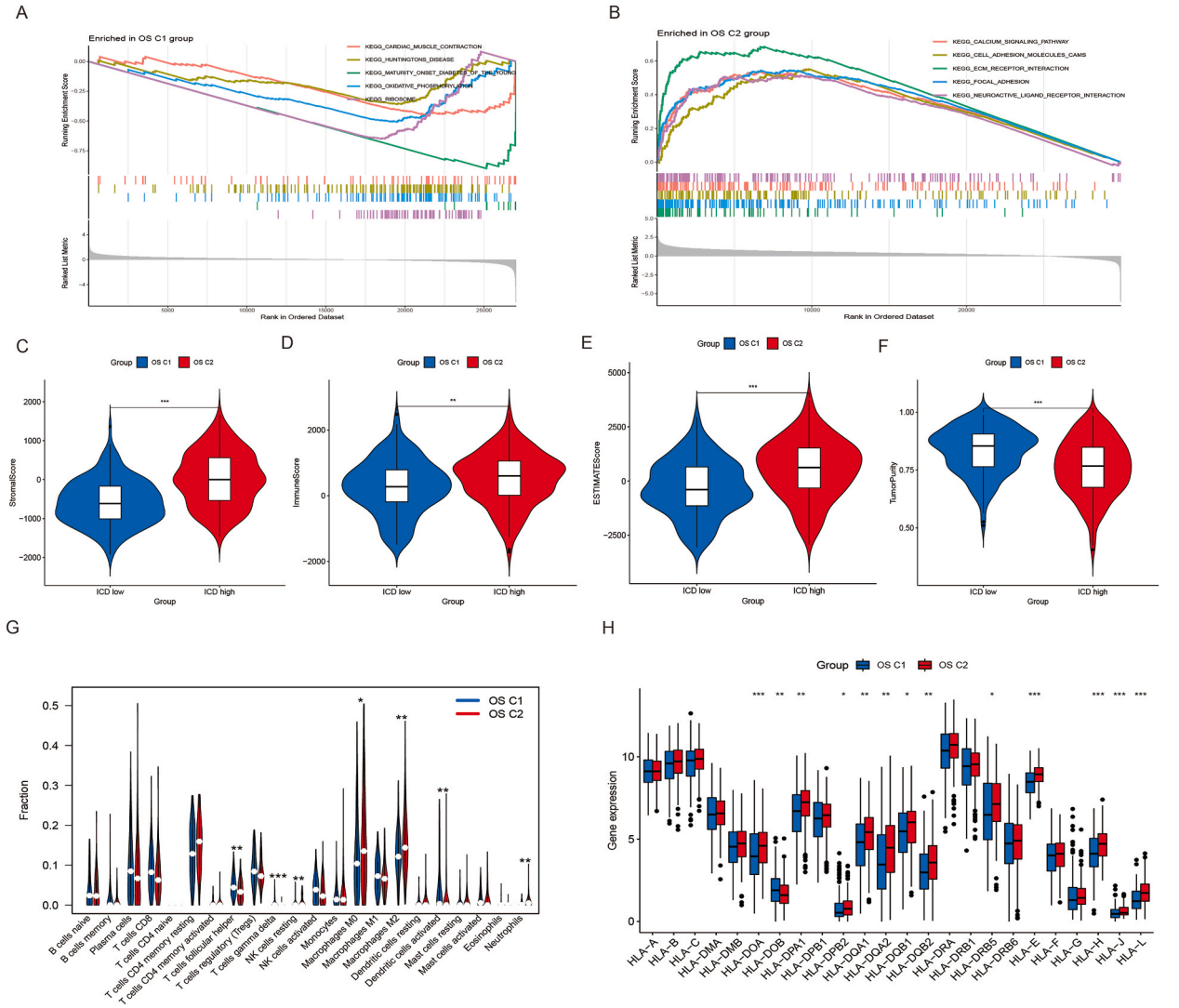


**Fig. 3.** Difference analysis of immune landscape characteristics and immune checkpoints between OS C1 and OS C2. (A) Myocardial contraction, Hun'ington's disease, juvenile mature diabetes, oxidative phosphorylation, ribosome and other pathways are significantly enriched in the OS C1 group. (B) The calcium signal pathway, cell adhesion molecule cam, ECM receptor interaction, focal adhesion and neural active ligand receptor interaction were significantly enriched in the OS C2 group. (C–F) Stromal score, immune score, estimated score and tumor purity analysis between OS C1 and OS C2. C: Stromal score; D: Immune score; E: Estimated score; F: Tumor purity. (G) Difference analysis of 22 kinds of immune cells between two OS subgroups. (H) Differential analysis of 13 HLA gene expression levels between 2 OS subgroups.

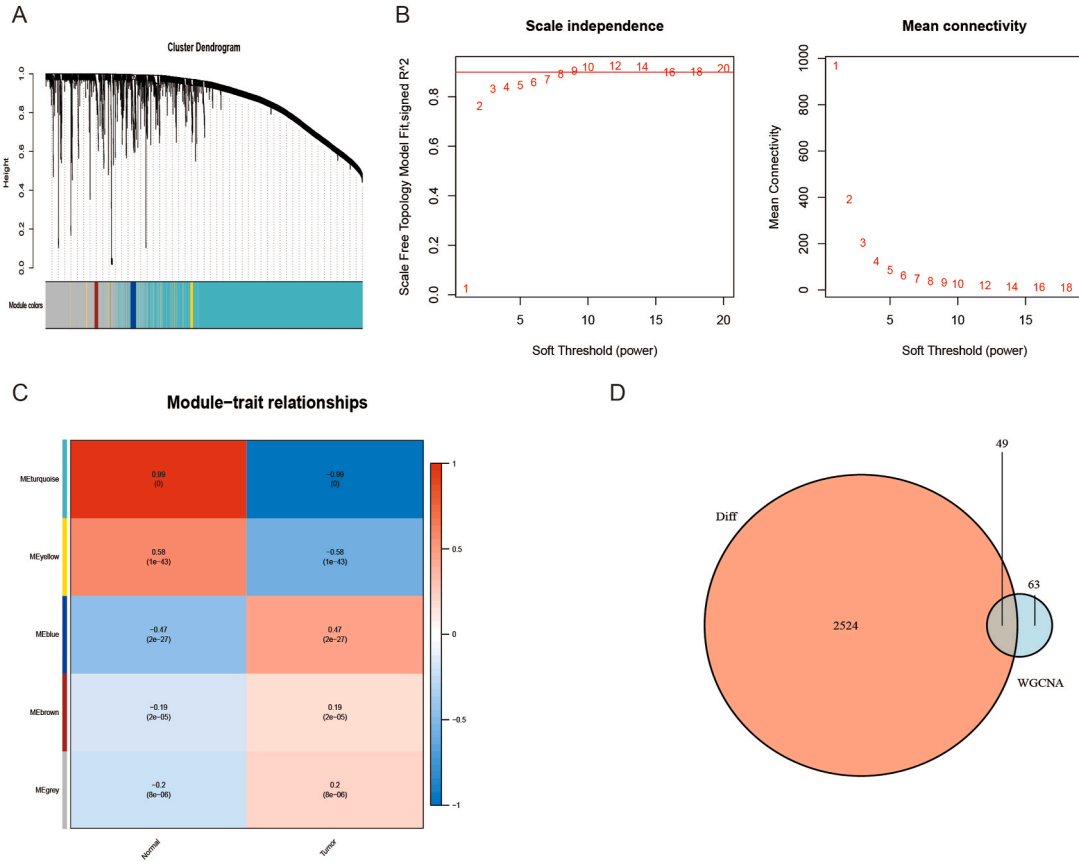


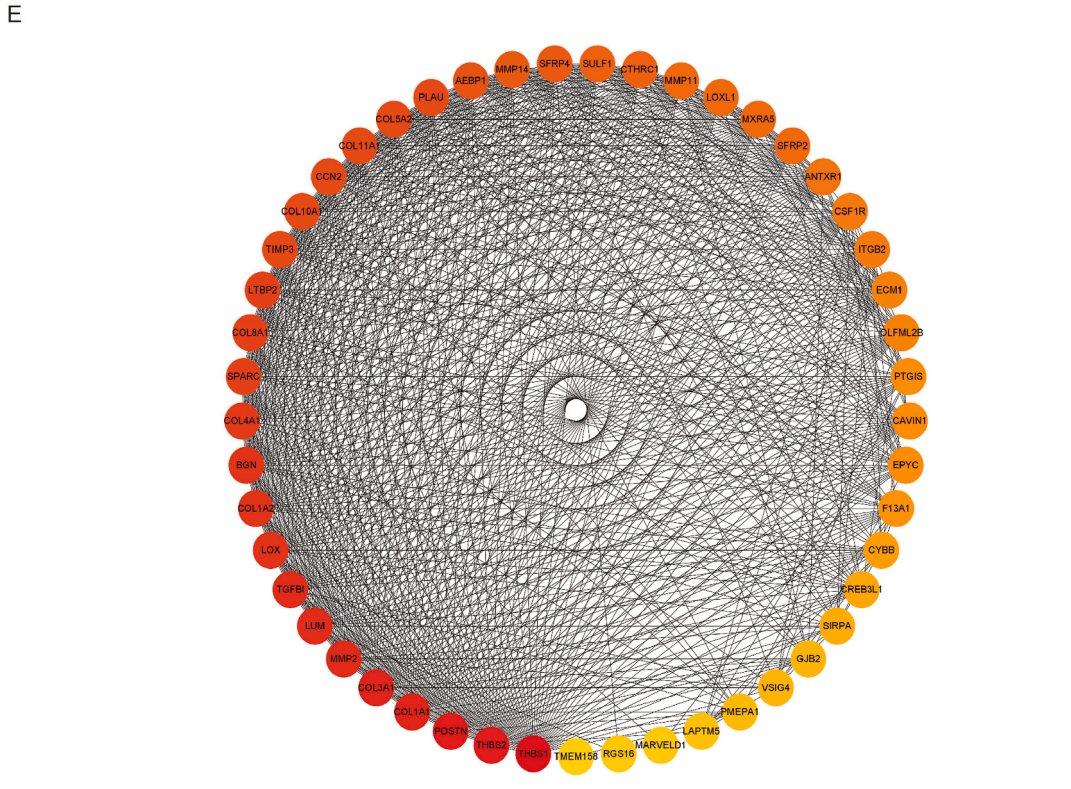


*(caption on next page)*

**Fig. 4.** WGCNA analysis in OV. (A) The sample tree diagram and clinical feature heat map are drawn. (B) The selection of soft threshold makes the scale-free topological index reach 0.80, and the average connectivity of 1–20 soft threshold power is analyzed. (C) A heat map of the correlation between the module and the OV. (D) Venn diagram shows the intersection genes between hub gene and DEGs. (E) Cytohubba obtained 49 hub genes connecting nodes.

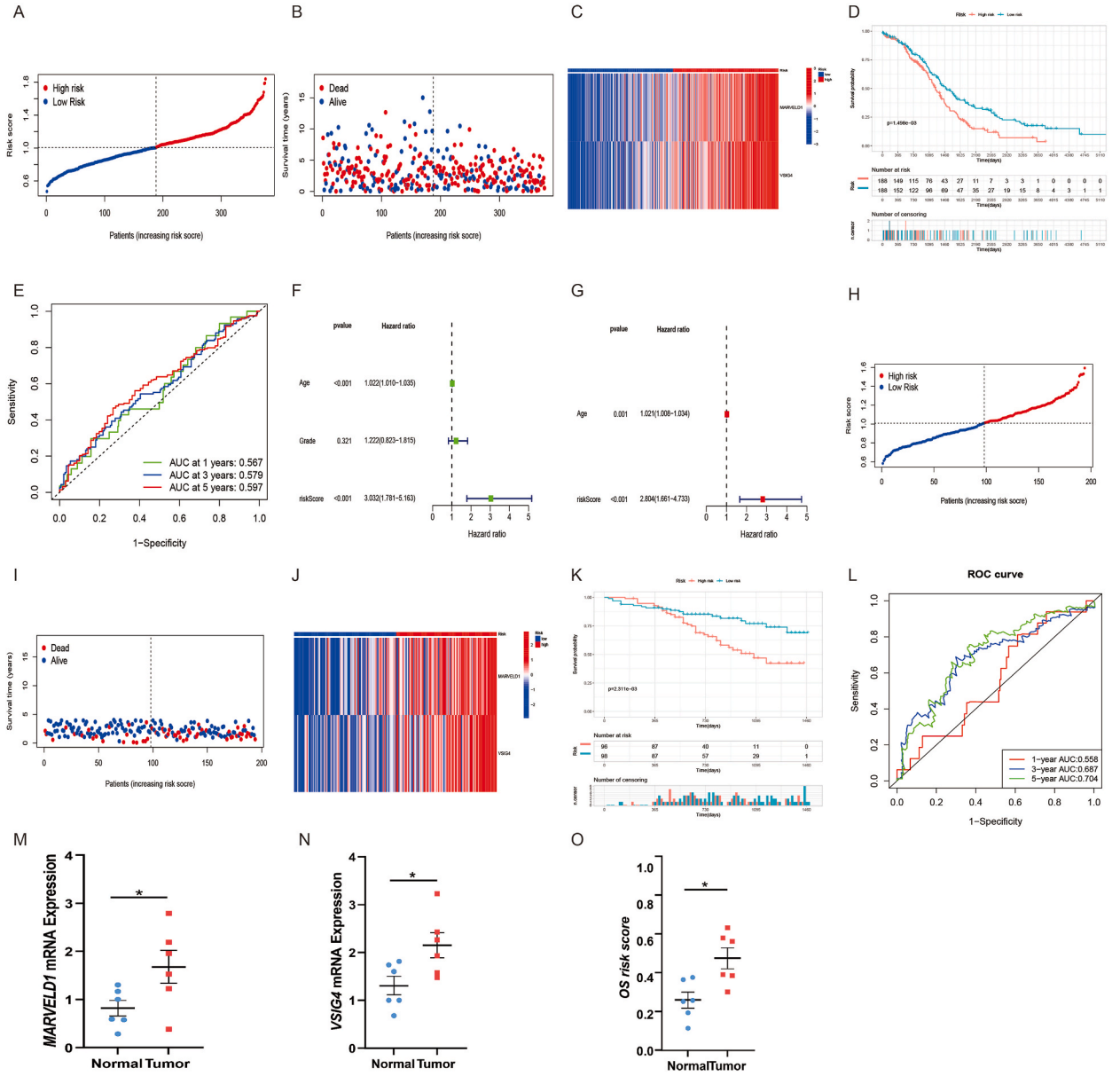


**Fig. 5.** Construction and validation of clinical prognosis model based on OS related characteristic genes. (A) The risk score based on the clinical prognosis model divides OV patients into high risk group and low risk group. (B) Survival status among OV patients in different risk groups. (C) The heat map shows the expression level of genes in the high risk group and the low risk group. (D) Survival differences between high-risk and low-risk groups. (E) ROC curve analysis predicted the total survival time of 1, 3 and 5 years in the training group. (F–G) univariate and multivariate Cox regression analysis suggested that the risk score of the clinical model could be used as an independent predictor. In the GEO cohort, (H) OV patients were divided into high-risk group and low-risk group based on the risk score of clinical prognosis model. (1) Survival status of OV patients between high-risk and low-risk groups. (J) The heat map shows the expression level of genes in the high risk group and the low risk group. (K) Survival differences between high-risk and low-risk groups. (50) ROC curve analysis predicted the total survival time of 1, 3 and 5 years in the training group. (M) PCR results of MARVELD1. (N) PCR results of VSIG4. (O) Results of OS risk score. *$p < 0.05$.

scores ($P < 0.001$) in the OS C1 group were lower than in the OS C2 group (Fig. 3C–E); also, the tumor purity in the OS C2 group was higher than in the OS C1 group ($P < 0.001$) (Fig. 3F). The proportion of 22 invasive immune cells was compared between both OS categories. The results of this comparison revealed that the levels of gamma-delta (γδ) T cells ($P < 0.001$), resting natural killer (NK) cells ($P < 0.01$), follicular helper T cells ($P < 0.01$), activated dendritic cells ($P < 0.01$), macrophages M0 ($P < 0.05$), macrophages M2 ($P < 0.01$), and neutrophils ($P < 0.01$) were significantly different in both OS categories (Fig. 3G). More importantly, the expression of 13 human leukocyte antigen (HLA) genes was found to differ significantly in both OS categories (Fig. 3H).

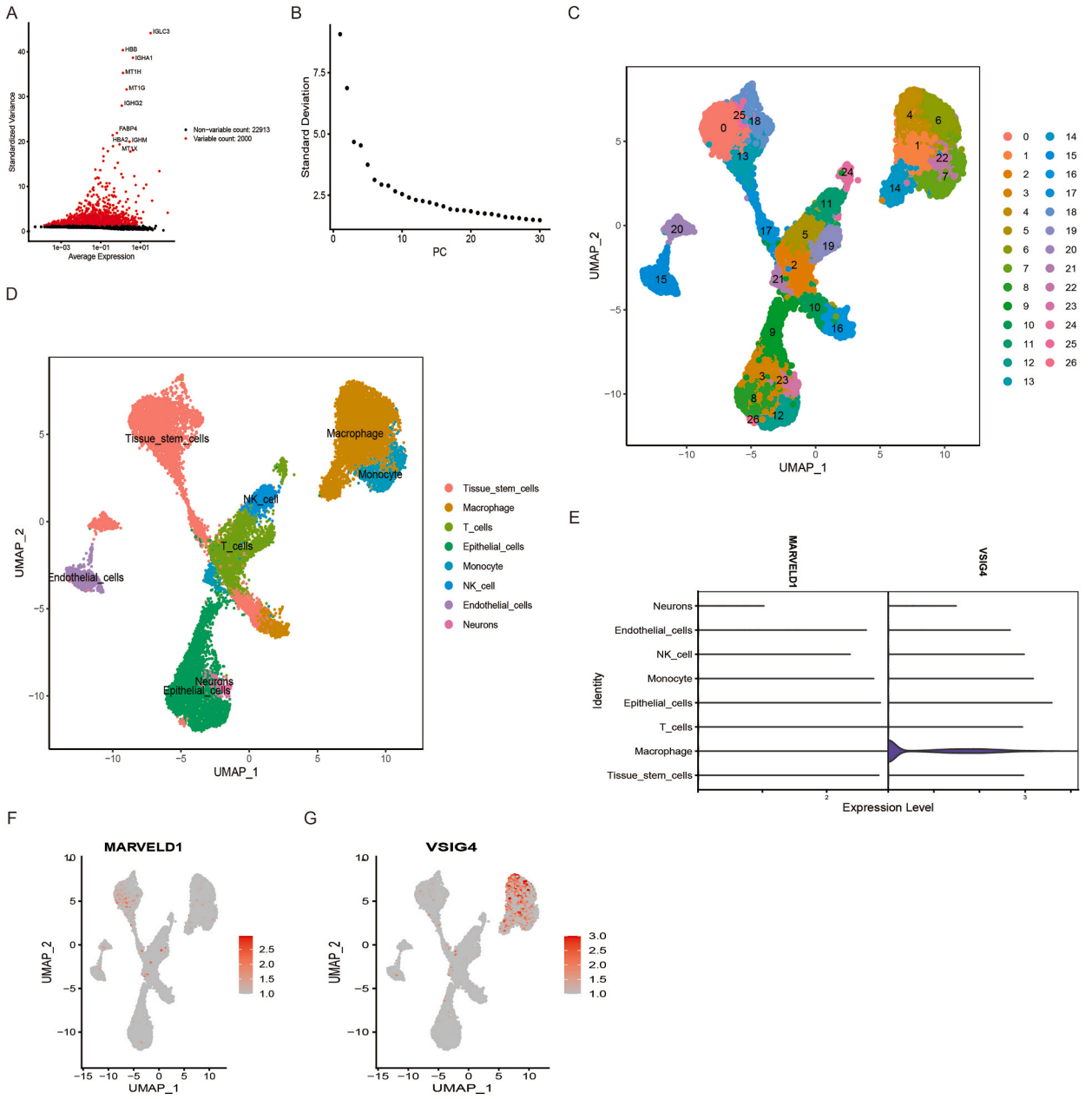


**Fig. 6.** Results of single-cell analysis showing the correlation of MARVELD1 and VSIG4 with the tumor microenvironment. (A) Genes were expressed in all samples. Red dots indicate the top 2000 highly variable genes in gene expression. (B) ElbowPlot plot. (C) UMAP cluster analysis plot showing the samples were categorized into 27 cell clusters. (D) 27 cell clusters annotated as eight immune cell clusters. (E) Expression levels of MARVELD1 and VSIG4 in the eight immune cell clusters. (F) Scatter plot of MARVELD1 expression in eight immune cell clusters. (G) Scatter plot of VSIG4 expression in eight immune cell clusters. (For interpretation of the references to colour in this figure legend, the reader is referred to the Web version of this article.)

### 3.4. WGCNA analysis and identification of core modules and core genes, and determination of OS-related characteristic genes

The WGCNA analysis was used to identify five co-expression modules. The blue module had the highest correlation (cor = 0.47, $p < 0.001$) of these 5 modules (Fig. 4A–C). While the blue module contained 66 hub genes, the brown module had 46 hub genes. A total of these 112 hub genes were selected for subsequent analysis. The intersection of the hub genes and the earlier DEGs were analyzed, and a total of 49 OS-related characteristic genes were identified (Fig. 4D). To investigate the biological significance of the 49 OS-related characterized genes, we constructed a PPI network graph using the STRING online database and Cytoscape software, and calculated the degree of each gene using Cytohubba, and scored the gene network and ranked the 49 genes with scores (Fig. 4E).

### 3.5. Constructing and validating the clinical prognosis model

The univariate regression analysis was conducted based on 49 OS-related characteristic genes. A total of 9 OS characteristic genes

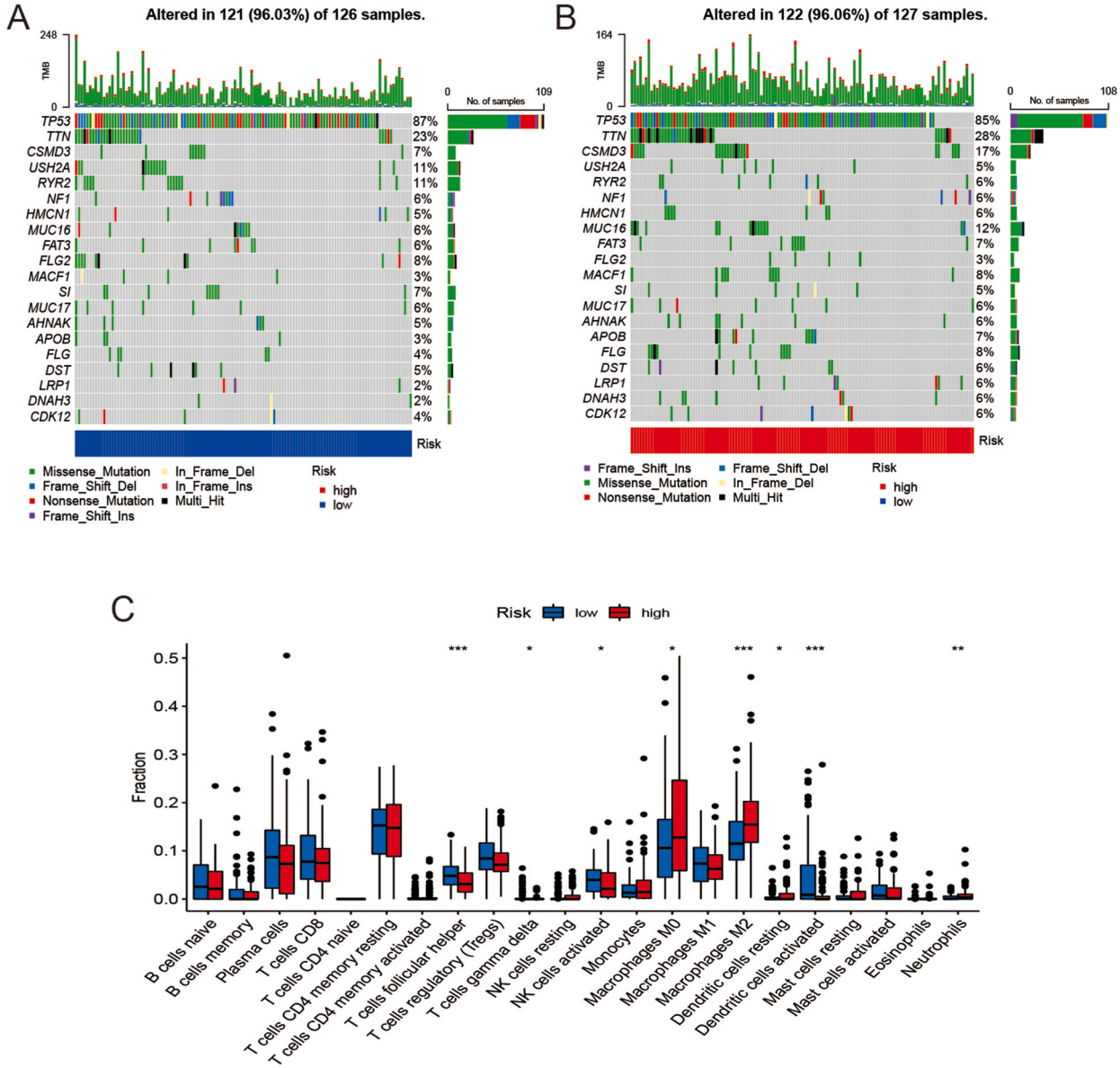


**Fig. 7.** Correlation between risk score of clinical prognosis model and somatic mutation and immune cells. (A, B) The waterfall diagram of tumor somatic mutation established between patients in high-risk group and low-risk group. Each upper bar graph shows TMB, and the number on the right represents the mutation frequency of each gene. These columns represent individual patients. A: Low risk group; B: High risk group. (C) There were significant differences in immune cells between high and low risk groups.

related to prognosis were identified. Finally, the multivariate regression model was used to construct a clinical prognosis model based on two OS-related characteristic genes. The following formula of the clinical prognosis model was used: OS risk score = (the gene expression of *MARVELD1* * 0.1527) + (the gene expression of *VSIG4* * 0.1145)

Patients with OV in the TCGA-OV dataset were classified into high-risk and low-risk groups depending on their median risk value from the clinical prognostic model (Fig. 5A). Fig. 5B shows the OS status of patients with OV in both risk groups. The expression levels of OS-related characteristic genes used to build clinical prognostic models in the low- and high-risk groups are presented in the heatmap (Fig. 5C). The survival analysis results implied that the OS status of low-risk patients was better than that of high-risk patients (Fig. 5D). The AUC values over 1, 3, and 5 years were 0.567, 0.579, and 0.597, respectively. These findings indicated that the clinical prognosis model showed a qualified predictive effect (Fig. 5E). According to the univariate and multivariate regression analyses, the novel clinical prognostic model could serve as an independent prognostic factor for patients with OV (Fig. 5F and G). More importantly, the results obtained from the validation group were in agreement with those obtained from the training group. Patients with OV belonging to the GEO dataset were categorized into high- and low-risk groups based on their median risk values derived from the clinical prognostic model (Fig. 5H). Fig. 5I shows the survival status of low-risk and high-risk patients. The expression levels of OS-related characteristic genes used to build clinical prognostic models in both the risk groups are presented in a heatmap (Fig. 5J). The results of the survival analysis implied that the OS status of the high-risk group was lower than that of the low-risk group (Fig. 5K). The ROC curves confirmed that the newly built clinical prognostic model had a good predictive ability. The AUC values for 1, 3, and 5 years were 0.558, 0.687, and 0.704, respectively (Fig. 5L). In addition, we validated the mRNA expression of the genes used to construct the model by qRT-PCR, and the results showed that the expression of MARVELD1 and VSIG4 was significantly upregulated in OV (Fig. 5M and N). The risk scores in tumor samples were significantly higher than those in normal samples (Fig. 5O).

### 3.6. Single-cell data analysis of the correlation of model-building genes with the tumor microenvironment

To further elucidate the correlation of MARVELD1 and VSIG4 with the tumor microenvironment of OV, we performed single-cell data analysis. After quality control, we selected the top 2000 highly variable genes for PCA analysis and downscaled the data (Fig. 6A). We categorized the samples into 17 different PCs according to ElbowPlot (Fig. 6B). During the downscaling phase of the UMAP algorithm, the samples ended up in 27 different cell clusters (Fig. 6C). The 27 cell clusters were further annotated into eight immune cell clusters (Fig. 6D). Fig. 6E shows the expression levels of MARVELD1 and VSIG4 in the different immune cell clusters. MARVELD1 is significantly expressed mainly in the Tissue stem cells cluster (Fig. 6F). VSIG4 is significantly expressed mainly in macrophage clusters (Fig. 6G).

### 3.7. Differential analysis of somatic mutation, immune cells, and immune checkpoint genes among different risk groups

This study employed the “maftools” software to analyze variations in the distribution of somatic mutations among the two risk groups derived from the TCGA-OV dataset. The tumor mutation burden (TMB) was greater in the high-risk patients than in the low-risk patients (Fig. 7A and B). The relationship between the clinical prognosis model and immune infiltration was analyzed based on the CIBERSORT values. The findings of this analysis revealed significant differences in the levels of macrophages M2, follicular helper T cells, activated dendritic cells, and neutrophils in both risk groups. For the results of immune cell infiltration, we found that the number of common killer immune cells was stronger in both the low-risk group than in the high-risk group. In the high-risk group, we observed elevated numbers of common immunosuppressive cells such as M2 macrophages, resting dendritic cells, suggesting to us that the poor prognosis in the high-risk group may be associated with extensive immunosuppression in the tumor (Fig. 7C). When compared to the high-risk patients, the low-risk group had a higher expression of dendritic cells activated and follicular helper T cells. More €mportantly, the low-risk patients from the CTLA4 treatment group were more likely to respond to immunotherapy (Fig. 8A–D).

## 4. Discussion

OV is a highly prevalent and fatal gynecologic malignancy that claims more than 150,000 lives worldwide each year [30]. Unfortunately, there has been no significant improvement in the survival rate of OV as compared to other cancers [1]. Several studies

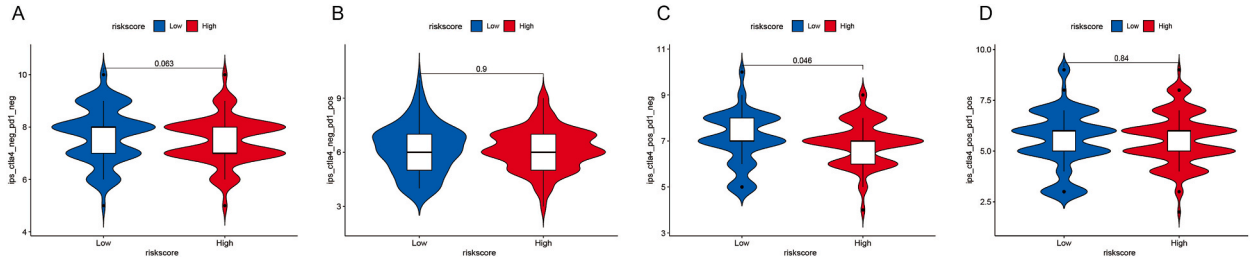


**Fig. 8.** Prediction of the effect of immunotherapy by risk score. (A) Non immunotherapy group. (B) PD-1 treatment group. (C) CTLA4 treatment group. (D) PD-1 and CTLA4 combined treatment group.

have demonstrated that OS plays a significant role in OV pathogenesis by mediating genetic modifications and signaling pathways. MiRNAs are crucial immune system mediators because they are involved in multiple inflammatory processes and are closely linked to disease progression and management [31,32]. Previous research has shown that OS can induce microRNA (miR)-141 and miR-200s-related overexpression, increasing the sensitivity of OV cells to paclitaxel and enhancing mesenchymal-epithelial cell transformation [33,34]. The Keap1-Nrf2-ARE pathway is one of the most crucial signaling pathways for cells to respond to OS. The Nrf2 pathway maintains the stability of a healthy genome and ovarian cell environment while inhibiting OS-induced carcinogenesis [35]. Furthermore, the Nrf2 pathway can protect OV cells from oxidative damage and help them resist several cytotoxic medicines, increasing OV cell invasiveness and resistance to chemotherapy [36–38]. However, the potential role of OS in the development of OV needs further research.

In this study, the OS gene-based unsupervised cluster analysis was used to establish two subtypes of OS, namely OS C1 and OS C2. It was found that the OS C1 subtype was significantly associated with myocardial contraction, Huntingto''s disease, juvenile diabetes mellitus, oxidative phosphorylation, ribosome, and other pathways. The subtype OS C2, on the other hand, was significantly related to the calcium signaling pathway, CAM, focal adhesion, ECM receptor interaction, and neural active ligand-receptor interaction. The focal adhesion kinase (FAK) is a non-receptor tyrosine kinase, which is involved in cellular or focal adhesion. Many studies have shown that FAK promotes cancer invasion and metastasis and is associated with poor clinical outcomes [39,40]. It may also be involved in protecting OV cells from nest loss and apoptosis, promoting OV progression [41,42]. Choe et al. demonstrated that curcumin can block β1 integrin stabilization, thereby inhibiting the activation of FAK and EGFR, to effectively inhibit the Rab coupling protein (RCP)-induced invasion of OV cancer cells [43]. According to our findings, the focal adhesion pathway was significantly enriched in the OS C2 group and showed an upward trend. This could possibly explain the shorter overall survival of patients in the OS C2 group than those in the OS C1 group. The results of the study also showed that the expression of M2 macrophage was higher in OS C2 than in OS C1. Tumor-associated macrophages (TAM) promote tumor growth by stimulating angiogenesis and enhancing tumor cell invasion, migration, and metastasis. FAK induces TAM by recruiting macrophages to tumor tissues and may exert tumor-promoting functions by regulating the expression of downstream genes [44].

In their study, Chen et al. demonstrated that pCa-derived CCN3 can differentiate macrophages into M2 phenotype and then recruit macrophages to produce the angiogenic vascular endothelial growth factor (VEGF). The FAK/Akt/NF–B signal transduction in M2 macrophages mediates VEGF synthesis and CCN3-induced angiogenesis [45]. The relationship between FAK and macrophages may be influenced similarly in OV, thereby accelerating its progression.

Here, a novel clinical prognosis model containing two OS-related characteristic genes (i.e., *MARVELD1*, *VSIG4*) was constructed. Our clinical prognostic model allows us to categorize patients into low-risk and high-risk groups, with patients in the low-risk group having a better survival advantage. Univariate and multivariate regression analyses have shown that both age and risk score can be used as independent prognostic factors for patients with OV. OV is primarily a disease of postmenopausal women, as more than 80% of cases are diagnosed in women over 50 years of age. Altered hormone levels, including estrogen, after menopause have been implicated in the etiology of OV [46–48]. Certainly, the risk score is more statistically significant than age. In addition, low-risk patients are better able to benefit from CTLA4 therapy. This suggests that our clinical prognostic model can accurately stratify and predict the survival outcomes of OV patients with precision and guide the personalized clinical dosing of patients. VSIG4 is a complement receptor of the well-known immunoglobulin (Ig) superfamily (CRIg). As a macrophage-specific immunomodulator, VSIG4 is an effective co-inhibitory ligand that strongly inhibits cytokine production and T-cell proliferation [49]. Previous studies have demonstrated that *VSIG4* is up-regulated in several types of cancers that occur in humans [50–52]. Moreover, tumor growth has been observed to be significantly suppressed in VSIG4-deficient mice [50]. A study by Jung Mi Byun et al. found that VSIG4 was highly expressed in OV compared to benign tumors. Soluble VSIG4 levels were significantly associated with progression and recurrence of OV [52]. The *MARVELD1* gene is a member of the MARVEL family and plays a role in membrane connectivity and vesicular transport [53]. Several studies have shown that the expression of *MARVELD1* is attenuated in a variety of cancers, including breast cancer, cervical cancer, and prostate cancer [54,55]. However, Alves et al. noted that *MARVELD1* was overexpressed in colon cancer [56]. Xia et al. also demonstrated that up-regulation of the MARVELD1 protein had a tumor-promoting effect on the malignant phenotype of glioma cancer cells, via the activation of the JAK/STAT signaling pathway [57]. Haoxiu Sun et al. reported that MARVELD1 modulates the genotoxic stress response in cancer cells, which is significantly associated with poor patient prognosis. PARP1 is a key enzyme with multiple functions involved in the DNA damage response and cell survival in cancer cells. The combination of MARVELD1 and PARP1 induces the combination of 5-FU and Olaphani for colon cancer drug resistance [58]. Upregulation of MARVELD1 expression is associated with increased chemosensitivity of hepatocellular carcinoma cells to epirubicin and 10-hydroxycamptothecin [59]. Downregulation of MARVELD1 expression inhibits resistance to paclitaxel and cisplatin in lung cancer cells [60]. In OV, upregulation of MARVELD1 protein expression increases chemotherapeutic resistance to the combination therapy of platinum and paclitaxel. combination therapy chemoresistance [61]. Since much remains unknown about the potential role of MARVELD1 and VSIG4 in OV, more research in this area is needed.

Drug resistance is a key challenge in OV therapy. Distinguishing between drug-resistant populations is essential to achieve personalized therapeutic treatment. Auranofin (AF) is a linear Au(I) complex containing an Au–S bond [62]. The anti-inflammatory and anticancer capabilities of AF have long been investigated. AF is currently being used in clinical trials for the treatment of chronic lymphocytic leukemia, lung and ovarian cancer. In OV, previous studies have demonstrated that AF helps to overcome resistance to cisplatin-based drugs [63–65]. Schuh et al. have also demonstrated that the antiproliferative properties of AF in cisplatin-sensitive and cisplatin-resistant human OC cells are reflected primarily through direct inhibition of the TrxR enzyme [65]. Importantly, the synergy of AF effects is enhanced when AF is combined with other compounds [66,67]. Unfortunately, studies on the role of AF in OV are still scarce, which requires more in-depth research.

There are still some shortcomings in this study. First, the results of the study were only validated by PCR. Second, the relatively small sample size of this study may have an impact on the generality of the results. We need to collect a larger sample size as a validation set to confirm the applicability and accuracy of the model. Finally, some clinicopathologic features were missing in the samples collected in this study; therefore, we also need to evaluate more clinicopathologic features, such as STAGE staging and TNM staging, to explore the impact of other potential mechanisms on survival.

## 5. Conclusion

In a nutshell, this study fills the gap in research on the mechanism of OS in OV. The clinical prognosis model constructed in this study has good predictive value for predicting the survival outcome of patients with OV. We believe that this study will provide valuable insights for improving the current treatment strategies of OV.

## Ethics approval and consent to participate

The experimental protocol was established, according to the ethical guidelines of the Helsinki Declaration and was approved by the Ethics Committee of Affiliated Hospital of Nantong University (2023-L123). Each participant provided the written informed consent for participation.

## Footnotes

Ethics approval and consent to participate. Not applicable.
Consent for publication. Not applicable.

## Funding

None.

## Availability of data and materials

Not applicable.

## CRediT authorship contribution statement

**Li Li:** Writing – original draft, Conceptualization. **Weiwei Zhang:** Writing – original draft, Data curation. **Yanjun Sun:** Writing – original draft, Data curation. **Weiling Zhang:** Methodology, Data curation. **Mengmeng Lu:** Methodology, Formal analysis. **Jiaqian Wang:** Validation, Software. **Yunfeng Jin:** Writing – review & editing, Writing – original draft. **Qinghua Xi:** Writing – review & editing, Supervision, Conceptualization.

## Declaration of competing interest

The authors declare that they have no known competing financial interests or personal relationships that could have appeared to influence the work reported in this paper.

## Acknowledgments

Not applicable.

## Appendix ASupplementary data

Supplementary data to this article can be found online at https://doi.org/10.1016/j.heliyon.2024.e28442.

## References

[1] R.L. Siegel, K.D. Miller, A. Jemal, Cancer statistics, 2019, CA A Cancer J. Clin. 69 (1) (2019) 7–34.
[2] P.M. Webb, S.J. Jordan, Epidemiology of epithelial ovarian cancer, Best Pract. Res. Clin. Obstet. Gynaecol. 41 (2017) 3–14.
[3] R. Thapa, O. Afzal, G. Gupta, et al., Unveiling the connection: long-chain non-coding RNAs and critical signaling pathways in breast cancer, Pathol. Res. Pract. 249 (2023) 154736.
[4] W. Chen, R. Zheng, P.D. Baade, et al., Cancer statistics in China, 2015, CA A Cancer J. Clin. 66 (2) (2016) 115–132.
[5] Z. Ďuračková, Some current insights into oxidative stress, Physiol. Res. 59 (4) (2010) 459–469.

[6] S. Reuter, S.C. Gupta, M.M. Chaturvedi, B.B. Aggarwal, Oxidative stress, inflammation, and cancer: how are they linked? Free Radic. Biol. Med. 49 (11) (2010) 1603–1616.
[7] Q. Wang, W. Guo, B. Hao, et al., Mechanistic study of TRPM2-Ca(2+)-CAMK2-BECN1 signaling in oxidative stress-induced autophagy inhibition, Autophagy 12 (8) (2016) 1340–1354.
[8] P. Bhatt, V. Kumar, V. Subramaniyan, et al., Plasma modification techniques for natural polymer-based drug delivery systems, Pharmaceutics 15 (8) (2023).
[9] S. Mukherjee, S. Nag, N. Mukerjee, et al., Unlocking exosome-based theragnostic signatures: deciphering secrets of ovarian cancer metastasis, ACS Omega 8 (40) (2023) 36614–36627.
[10] J.D. Hayes, A.T. Dinkova-Kostova, K.D. Tew, Oxidative stress in cancer, Cancer Cell 38 (2) (2020) 167–197.
[11] N. Rajan, S. Debnath, K. Perveen, et al., Optimizing hybrid vigor: a comprehensive analysis of genetic distance and heterosis in eggplant landraces, Front. Plant Sci. 14 (2023) 1238870.
[12] F.A. Rizwi, M. Abubakar, E.R. Puppala, et al., Janus kinase-signal transducer and activator of transcription inhibitors for the treatment and management of cancer, J. Environ. Pathol. Toxicol. Oncol. : official organ of the International Society for Environmental Toxicology and Cancer 42 (4) (2023) 15–29.
[13] V. Sosa, T. Moliné, R. Somoza, R. Paciucci, H. Kondoh, L.L. Me, Oxidative stress and cancer: an overview, Ageing Res. Rev. 12 (1) (2013) 376–390.
[14] S. Kumari, A.K. Badana, M.M. G, S. G, R. Malla, Reactive oxygen species: a key constituent in cancer survival, Biomark. Insights 13 (2018) 1177271918755391.
[15] C.A. Caneba, L. Yang, J. Baddour, et al., Nitric oxide is a positive regulator of the Warburg effect in ovarian cancer cells, Cell Death Dis. 5 (6) (2014) e1302.
[16] S. Galadari, A. Rahman, S. Pallichankandy, F. Thayyullathil, Reactive oxygen species and cancer paradox: to promote or to suppress? Free Radic. Biol. Med. 104 (2017) 144–164.
[17] S. Singh, Sharma N. Hema, et al., Focusing the pivotal role of nanotechnology in Huntington's disease: an insight into the recent advancements, Environ. Sci. Pollut. Res. Int. 29 (49) (2022) 73809–73827.
[18] T. Amano, A. Murakami, T. Murakami, T. Chano, Antioxidants and therapeutic targets in ovarian clear cell carcinoma, Antioxidants 10 (2) (2021).
[19] S. Shigeta, M. Toyoshima, K. Kitatani, M. Ishibashi, T. Usui, N. Yaegashi, Transferrin facilitates the formation of DNA double-strand breaks via transferrin receptor 1: the possible involvement of transferrin in carcinogenesis of high-grade serous ovarian cancer, Oncogene 35 (27) (2016) 3577–3586.
[20] S.Z. Safi, L. Saeed, H. Shah, et al., Mechanisms of β-adrenergic receptors agonists in mediating pro and anti-apoptotic pathways in hyperglycemic Müller cells, Mol. Biol. Rep. 49 (10) (2022) 9473–9480.
[21] V. Subramaniyan, S. Fuloria, G. Gupta, et al., A review on epidermal growth factor receptor's role in breast and non-small cell lung cancer, Chem. Biol. Interact. 351 (2022) 109735.
[22] G.M. Saed, M.P. Diamond, N.M. Fletcher, Updates of the role of oxidative stress in the pathogenesis of ovarian cancer, Gynecol. Oncol. 145 (3) (2017) 595–602.
[23] D.N. Ding, L.Z. Xie, Y. Shen, et al., Insights into the role of oxidative stress in ovarian cancer, Oxid. Med. Cell. Longev. 2021 (2021) 8388258.
[24] J.T. Leek, W.E. Johnson, H.S. Parker, A.E. Jaffe, J.D. Storey, The sva package for removing batch effects and other unwanted variation in high-throughput experiments, Bioinformatics 28 (6) (2012) 882–883.
[25] J.T. Leek, R.B. Scharpf, H.C. Bravo, et al., Tackling the widespread and critical impact of batch effects in high-throughput data, Nat. Rev. Genet. 11 (10) (2010) 733–739.
[26] G. Yu, L.G. Wang, Y. Han, Q.Y. He, clusterProfiler: an R package for comparing biological themes among gene clusters, Omics-a Journal of Integrative Biology 16 (5) (2012) 284–287.
[27] P. Langfelder, S. Horvath, WGCNA: an R package for weighted correlation network analysis, BMC Bioinf. 9 (2008) 559.
[28] D. Szklarczyk, A.L. Gable, K.C. Nastou, et al., The STRING database in 2021: customizable protein-protein networks, and functional characterization of user-uploaded gene/measurement sets, Nucleic Acids Res. 49 (D1) (2021) D605–d612.
[29] A. Mayakonda, D.C. Lin, Y. Assenov, C. Plass, H.P. Koeffler, Maftools: efficient and comprehensive analysis of somatic variants in cancer, Genome Res. 28 (11) (2018).
[30] S. Lheureux, M. Braunstein, A.M. Oza, Epithelial ovarian cancer: evolution of management in the era of precision medicine, CA A Cancer J. Clin. 69 (4) (2019) 280–304.
[31] S.M. Acuña, L.M. Floeter-Winter, S.M. Muxel, MicroRNAs: biological regulators in pathogen-host interactions, Cells 9 (1) (2020).
[32] R. Malviya, S. Jha, N.K. Fuloria, et al., Determination of temperature-dependent coefficients of viscosity and surface tension of tamarind seeds (Tamarindus indica L.) polymer, Polymers 13 (4) (2021).
[33] A. Brozovic, G.E. Duran, Y.C. Wang, E.B. Francisco, B.I. Sikic, The miR-200 family differentially regulates sensitivity to paclitaxel and carboplatin in human ovarian carcinoma OVCAR-3 and MES-OV cells, Mol. Oncol. 9 (8) (2015) 1678–1693.
[34] B. Mateescu, L. Batista, M. Cardon, et al., miR-141 and miR-200a act on ovarian tumorigenesis by controlling oxidative stress response, Nat. Med. 17 (12) (2011) 1627–1635.
[35] M.G. van der Wijst, C. Huisman, A. Mposhi, G. Roelfes, M.G. Rots, Targeting Nrf2 in healthy and malignant ovarian epithelial cells: protection versus promotion, Mol. Oncol. 9 (7) (2015) 1259–1273.
[36] R. Sirota, D. Gibson, R. Kohen, The role of the catecholic and the electrophilic moieties of caffeic acid in Nrf2/Keap1 pathway activation in ovarian carcinoma cell lines, Redox Biol. 4 (2015) 48–59.
[37] M.H. Xia, X.Y. Yan, L. Zhou, et al., p62 suppressed VK3-induced oxidative damage through keap1/Nrf2 pathway in human ovarian cancer cells, J. Cancer 11 (6) (2020) 1299–1307.
[38] N. Liu, X. Lin, C. Huang, Activation of the reverse transsulfuration pathway through NRF2/CBS confers erastin-induced ferroptosis resistance, Br. J. Cancer 122 (2) (2020) 279–292.
[39] M. Xia, H. Yu, S. Gu, et al., p62/SQSTM1 is involved in cisplatin resistance in human ovarian cancer cells via the Keap1-Nrf2-ARE system, Int. J. Oncol. 45 (6) (2014) 2341–2348.
[40] V.M. Golubovskaya, F.A. Kweh, W.G. Cance, Focal adhesion kinase and cancer, Histol. Histopathol. 24 (4) (2009) 503–510.
[41] A.K. Sood, G.N. Armaiz-Pena, J. Halder, et al., Adrenergic modulation of focal adhesion kinase protects human ovarian cancer cells from anoikis, J. Clin. Invest. 120 (5) (2010) 1515–1523.
[42] A.K. Mitra, K. Sawada, P. Tiwari, K. Mui, K. Gwin, E. Lengyel, Ligand-independent activation of c-Met by fibronectin and α(5)β(1)-integrin regulates ovarian cancer invasion and metastasis, Oncogene 30 (13) (2011) 1566–1576.
[43] S.R. Choe, Y.N. Kim, C.G. Park, K.H. Cho, D.Y. Cho, H.Y. Lee, RCP induces FAK phosphorylation and ovarian cancer cell invasion with inhibition by curcumin, Exp. Mol. Med. 50 (4) (2018) 1–10.
[44] Y.L. Tai, L.C. Chen, T.L. Shen, Emerging roles of focal adhesion kinase in cancer, BioMed Res. Int. 2015 (2015) 690690.
[45] P.C. Chen, H.C. Cheng, J. Wang, et al., Prostate cancer-derived CCN3 induces M2 macrophage infiltration and contributes to angiogenesis in prostate cancer microenvironment, Oncotarget 5 (6) (2014) 1595–1608.
[46] H.A. Risch, Hormonal etiology of epithelial ovarian cancer, with a hypothesis concerning the role of androgens and progesterone, J. Natl. Cancer Inst. 90 (23) (1998) 1774–1786.
[47] F. Mungenast, T. Thalhammer, Estrogen biosynthesis and action in ovarian cancer, Front. Endocrinol. 5 (2014) 192.
[48] Å. Johansson, D. Schmitz, J. Höglund, F. Hadizadeh, T. Karlsson, W.E. Ek, Investigating the effect of Estradiol levels on the risk of breast, endometrial, and ovarian cancer, Journal of the Endocrine Society 6 (8) (2022) bvac100.
[49] X. Zhou, S. Khan, D. Huang, L. Li, V-Set and immunoglobulin domain containing (VSIG) proteins as emerging immune checkpoint targets for cancer immunotherapy, Front. Immunol. 13 (2022) 938470.
[50] Y. Liao, S. Guo, Y. Chen, et al., VSIG4 expression on macrophages facilitates lung cancer development, Laboratory investigation; a journal of technical methods and pathology 94 (7) (2014) 706–715.
[51] L.A. Sturtz, B. Deyarmin, R. van Laar, W. Yarina, C.D. Shriver, R.E. Ellsworth, Gene expression differences in adipose tissue associated with breast tumorigenesis, Adipocyte 3 (2) (2014) 107–114.

[52] J.M. Byun, D.H. Jeong, I.H. Choi, et al., The significance of VSIG4 expression in ovarian cancer, in: International Journal of Gynecological Cancer : Official Journal of the International Gynecological Cancer Society, 2017, pp. 872–878, 27(5.
[53] W. Ma, H. Shen, Q. Li, et al., MARVELD1 attenuates arsenic trioxide-induced apoptosis in liver cancer cells by inhibiting reactive oxygen species production, Ann. Transl. Med. 7 (9) (2019) 200.
[54] S. Wang, Y. Li, F. Han, et al., Identification and characterization of MARVELD1, a novel nuclear protein that is down-regulated in multiple cancers and silenced by DNA methylation, Cancer Lett. 282 (1) (2009) 77–86.
[55] F. Martín-Belmonte, J.A. Martínez-Menárguez, J.F. Aranda, J. Ballesta, M.C. de Marco, M.A. Alonso, MAL regulates clathrin-mediated endocytosis at the apical surface of Madin-Darby canine kidney cells, J. Cell Biol. 163 (1) (2003) 155–164.
[56] P.M. Alves, N. Lévy, B.J. Stevenson, et al., Identification of tumor-associated antigens by large-scale analysis of genes expressed in human colorectal cancer, Cancer Immun. 8 (2008) 11.
[57] L. Xia, P. Jin, W. Tian, S. Liang, L. Tan, B. Li, Up-regulation of MARVEL domain-containing protein 1 (MARVELD1) accelerated the malignant phenotype of glioma cancer cells via mediating JAK/STAT signaling pathway, Brazilian journal of medical and biological research = Revista brasileira de pesquisas medicas e biologicas 54 (7) (2021) e10236.
[58] H. Sun, C. Liu, F. Han, et al., The regulation loop of MARVELD1 interacting with PARP1 in DNA damage response maintains genome stability and promotes therapy resistance of cancer cells, Cell Death Differ. 30 (4) (2023) 922–937.
[59] Y. Yu, Y. Zhang, J. Hu, et al., MARVELD1 inhibited cell proliferation and enhance chemosensitivity via increasing expression of p53 and p16 in hepatocellular carcinoma, Cancer Sci. 103 (4) (2012) 716–722.
[60] J. Li, H. Yan, L. Zhao, et al., Inhibition of SREBP increases gefitinib sensitivity in non-small cell lung cancer cells, Oncotarget 7 (32) (2016) 52392–52403.
[61] J.T. Fekete, Á. Ősz, I. Pete, G.R. Nagy, I. Vereczkey, B. Győrffy, Predictive biomarkers of platinum and taxane resistance using the transcriptomic data of 1816 ovarian cancer patients, Gynecol. Oncol. 156 (3) (2020) 654–661.
[62] A.E. Finkelstein, D.T. Walz, V. Batista, M. Mizraji, F. Roisman, A. Misher, Auranofin. New oral gold compound for treatment of rheumatoid arthritis, Ann. Rheum. Dis. 35 (3) (1976) 251–257.
[63] C. Marzano, V. Gandin, A. Folda, G. Scutari, A. Bindoli, M.P. Rigobello, Inhibition of thioredoxin reductase by auranofin induces apoptosis in cisplatin-resistant human ovarian cancer cells, Free Radic. Biol. Med. 42 (6) (2007) 872–881.
[64] T. Marzo, L. Massai, A. Pratesi, et al., Replacement of the thiosugar of auranofin with iodide enhances the anticancer potency in a mouse model of ovarian cancer, ACS Med. Chem. Lett. 10 (4) (2019) 656–660.
[65] E. Schuh, C. Pflüger, A. Citta, et al., Gold(I) carbene complexes causing thioredoxin 1 and thioredoxin 2 oxidation as potential anticancer agents, J. Med. Chem. 55 (11) (2012) 5518–5528.
[66] W. Fiskus, N. Saba, M. Shen, et al., Auranofin induces lethal oxidative and endoplasmic reticulum stress and exerts potent preclinical activity against chronic lymphocytic leukemia, Cancer Res. 74 (9) (2014) 2520–2532.
[67] H. Huang, Y. Liao, N. Liu, et al., Two clinical drugs deubiquitinase inhibitor auranofin and aldehyde dehydrogenase inhibitor disulfiram trigger synergistic anti-tumor effects in vitro and in vivo, Oncotarget 7 (3) (2016) 2796–2808.